ACS Catalysis

Research Article

Cite This: ACS Catal. 2020, 10, 1938−1946

pubs.acs.org/acscatalysis

Exploring the Origin of Amidase Substrate Promiscuity in CALB by a Computational Approach

Miquel À Galmés,[†] Eduardo García-Junceda,*[,‡] Katarzyna Świderek,*[,†] and Vicent Moliner*[,†]

[†]Departament de Química Física i Analítica, Universitat Jaume I, 12071 Castellón, Spain

[‡]Departamento de Química Orgánica Biológica, Instituto de Química Orgánica General, CSIC Juan de la Cierva 3, 28006 Madrid, Spain

Supporting Information

ABSTRACT: Enzyme promiscuity attracts the interest of the industrial and academic sectors because of its application in the design of biocatalysts. The amidase activity of *Candida antarctica* lipase B (CALB) on two different substrates has been studied by theoretical quantum mechanics/molecular mechanics methods, supported by experimental kinetic measurements. The aim of the study is to understand the substrate promiscuity of CALB in this secondary reaction and the origin of its promiscuous catalytic activity. The computational results predict activation free energies in very good agreement with the kinetic data and confirm that the activity of CALB as an amidase, despite depending on the features of the amide substrate, is dictated by the electrostatic effects of the protein. The protein polarizes and activates the substrate as well as stabilizes the transition state, thus enhancing the rate constant. Our results can provide guides for future designs of biocatalysts based on electrostatic arguments.

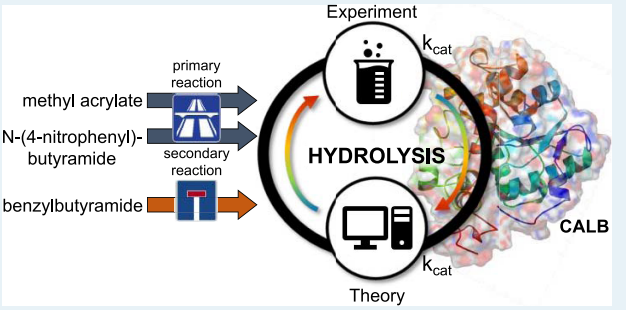

KEYWORDS: *computational chemistry, enzyme catalysis, enzyme promiscuity, QM/MM, molecular dynamics, free energy surfaces*

INTRODUCTION

Enzymes have evolved along millions of years to catalyze specific chemical transformations on specific type of substrates.[1] However, some enzymes conserve secondary activities other than the primary one, although their catalytic efficiency is almost always very poor compared to the primary reaction. This fact is due to the lack of the selective pressure over the evolution period.[2] The presence of these secondary reactions, known as catalytic promiscuity, can be the starting point for the evolution of enzymes in vivo,[3] which has become a very interesting field from the industrial and the academic points of view.[4−10] In addition, many enzymes show substrate promiscuity, which involves the ability to accept a range of different substrates. Having tools to enhance the rate constant of a secondary reaction on a particular substrate can be used to obtain high-value chemicals, which is nowadays of vital importance.[11,12] In addition, understanding the molecular basis of enzyme promiscuity is crucial for the rational design of new environmentally friendly catalysts.

It is reported that many lipases show promiscuous behavior,[4] and *Candida antarctica* lipase B (CALB) is one of the best well-known highly promiscuous enzyme. CALB's primary activity comprises the hydrolysis of the ester bond in triacylglycerides (Figure 1A), but it is also capable of catalyzing a plethora of different reactions such as the synthesis of esters and amides, transacylation of alcohols,[13] epoxidation reactions,[14] aldol additions, Michael-type additions,[4,15] among many others.[16]

As a carboxylic ester hydrolase, CALB performs its activity by a characteristic catalytic triad composed of Ser−His−Asp (Figure 1B). Here, the His224 residue has a very relevant role in the activity by acting as an acid/base residue during the full catalytic process. This acid/base character of histidine is governed by the aspartate residue that modulates its pK_a. Additionally, an oxyanion hole formed by the residues Thr40 and Gln106 is also present in the active site pocket. As confirmed by computational studies, this oxyanion hole has a double role: first, it is responsible for orienting the substrate in the active site, and second, it stabilizes the negative charge accumulated on the substrate during the hydrolysis.[18] The hydrolysis of ester natural substrates is proposed to be a four-step reaction[18] that involves, in the first step, the attack of the catalytic serine to the carbonyl carbon of the amide. In the second step, the release of the leaving group occurs as an effect of the acid−base character of His224. The products are released due to the hydrolysis of the acyl−enzyme complex in the third and the last chemical steps.

Among all of the secondary reactions that CALB is capable to catalyze, the hydrolysis of the amide bond has special interest (Figure 1A). This reaction is present ubiquitously in nature, from the proteolysis to the inhibition of some

Received: September 18, 2019
Revised: October 22, 2019
Published: November 1, 2019

DOI: 10.1021/acscatal.9b04002
ACS Catal. 2020, 10, 1938−1946

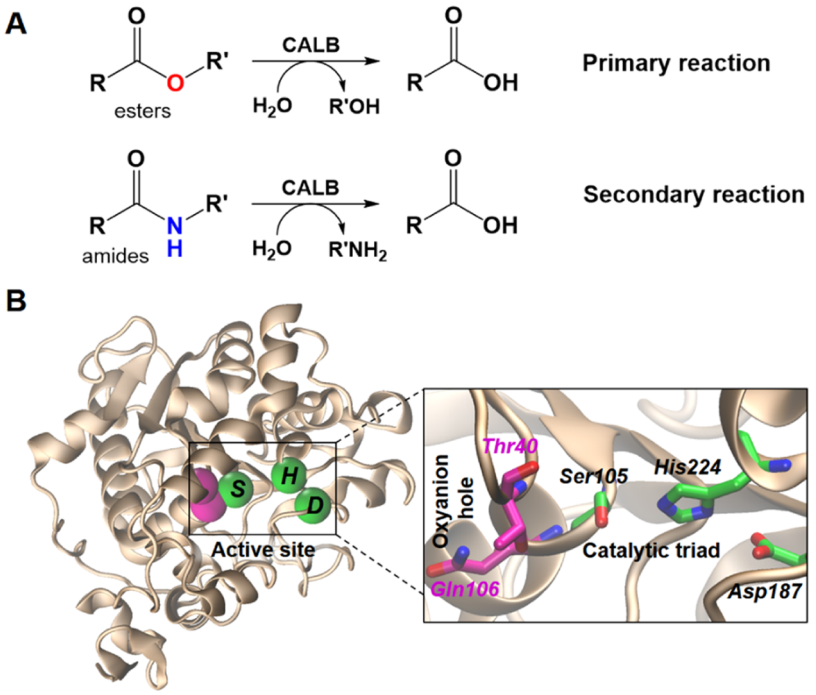

Figure 1. (A) General scheme of the primary and secondary reactions, ester and amide hydrolysis, catalyzed by CALB. (B) Crystal structure of CALB (PDB ID 1TCA)[17] together with the detail of the active site indicating the key residues.

antibiotics by the molecular machinery of pathogens.[19] CALB has been widely studied, rendering a significant amount of experimental data that is available in the literature.[4,5,20−22] In particular, the hydrolysis of the amide bond catalyzed by CALB was experimentally studied by López-Munguía and co-workers,[23] providing evidence that the enzyme is capable to hydrolyze the amides of several vanillyl derivatives. Obviously, the catalytic efficiency of the amidase reaction on these type of substrates is considerably lower than that of the native ester hydrolysis. Thus, CALB is an appropriate candidate that can serve as a good example to understand the origin of promiscuity in enzymes and to propose mutations that can enhance the rate constant of secondary reactions. The present work is focused on the study of the reaction mechanism of the hydrolysis of the amide bond carried out by CALB on two different substrates, combining experimental kinetic studies and theoretical quantum mechanics/molecular mechanics (QM/MM) methods. The description of the full reaction mechanism at atomistic level derived from the simulations sheds light on the substrate promiscuity of CALB in this secondary reaction, and on the origin of its catalytic activity. We believed that the obtained results will not only allow understanding its promiscuity but also exploring the possibility of using this protein as a scaffold to design new improved and more efficient biocatalysts.

COMPUTATIONAL METHODS

An initial equilibrated system was taken from a previous study on the primary reaction catalyzed by CALB,[18] prepared from the crystal structure available in the Protein Data bank under PDB ID 1TCA.[17] Further details of the setting up of the system are reported in the Supporting Information.

The amidase reaction was studied with two different substrates, benzylbutyramide (**1**) and *N*-(4-nitrophenyl)-butyramide (**2**). Compound **1** is a derivative of vanillyl with a short acyl chain of four carbons, which was proposed by López-Munguía and co-workers.[23] In **2**, the lone pair of the aniline nitrogen can be delocalized into the aromatic ring, making it a far weaker base and better leaving group compared to benzylamine where the nitrogen lone pair cannot delocalize due to the presence of an additional sp^3 carbon that, a priori, can increase the positive charge character on the anilide C1 compared to benzylamide. After equilibration of the systems by classical molecular dynamics (MD) simulations, the full system was partitioned into a QM and a MM region (see Figure 2). AM1[24] and M06-2X[25] Hamiltonians were selected to describe the QM region, while the OPLS-AA force field[26,27] was used to describe the residues of the protein (4625 atoms) and TIP3P[28] was the force field selected to describe the water molecules

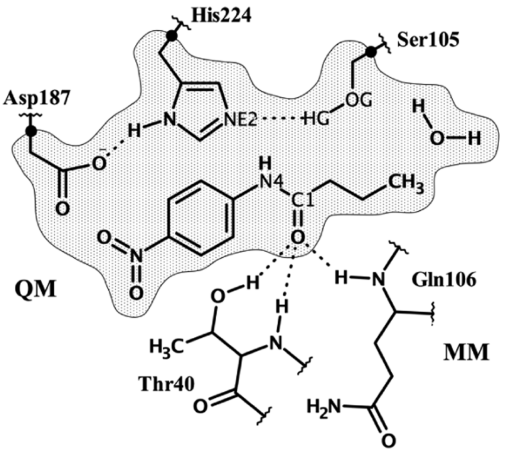

Figure 2. Schematic representation of the active site of CALB with substrate **2**. The QM region is represented as a shaded region. Black dots represent link atoms between QM and MM regions. The interaction between **2** and the oxyanion hole (Thr40 and Gln106) is shown as dashed lines.

DOI: 10.1021/acscatal.9b04002
ACS Catal. 2020, 10, 1938−1946

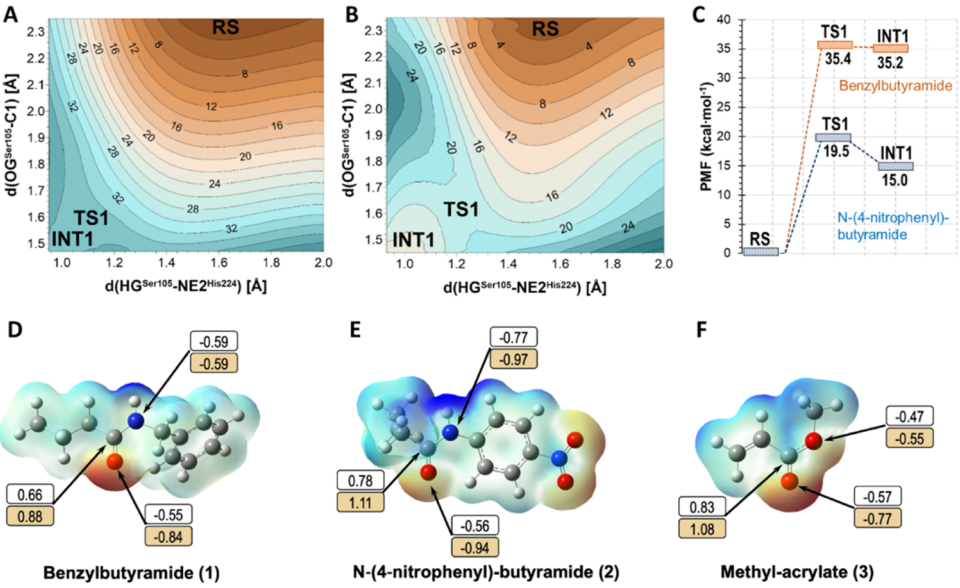

Figure 3. 2D-PMF of the first chemical step of the hydrolysis of **1** (A) and **2** (B) computed at the M06-2X:AM1/MM level. (C) Free energy profiles derived from the 2D-PMFs. Distances are in ångstroms, and energies of isoenergetic lines are in kcal mol^{-1}. Maps of electrostatic potential computed at the M06-2X/6-31+G** level in the gas phase for the two substrates of the CALB secondary reaction, **1** (D) and **2** (E), and for the substrate of the CALB primary reaction methyl acrylate (**3**) (F). Charge values in panels (D)−(F) (in au) were computed in the gas phase (white squares) and in the active site of the protein (brown squares).

(60 014 atoms). The standard 6-31+G(d,p) basis set was employed when the density functional theory (DFT) Hamiltonian was used to describe the QM subset of atoms. Hydrogen link atoms were placed in the QM−MM frontier bonds, as depicted in Figure 2.

QM/MM free energy surfaces (FESs) were obtained, in terms of two-dimensional potentials of mean force (2D-PMF),[29−31] for every step of the reaction using the umbrella sampling approach[29,32] combined with the weighted histogram analysis method (WHAM)[33] with the fDYNAMO library.[34] To correct the possible source of error derived from the low level of theory used to describe the QM region during the MD simulations, in this case, the AM1 semiempirical Hamiltonian, spline under tension corrections were used, based on the original work of Truhlar and co-workers.[35−37] As described in previous papers,[38,39] a correction term is interpolated to any value along the reaction coordinates in the FES based on multiple structures derived from the AM1/MM simulations. A continuous energy function is used to obtain the corrected PMFs using the hybrid M06-2X functional with the standard 6-31+G(d,p) basis set (see the Supporting Information for details). These calculations were carried out using the Gaussian09 program.[40]

Kinetic isotope effects (KIEs) were calculated, at M06-2X/MM and AM1/MM levels, from isotopic substitution of the key atoms in the reactants and the different transition state structures, as described in previous papers.[18,41,42] Details and further discussions are provided in the Supporting Information.

EXPERIMENTAL METHODS

Experimental kinetic studies in CALB were performed to evaluate the hydrolysis of the amide bond of both substrates. For that, compound **1** was synthetized using an enzymatic approach (see the Supporting Information for details). Briefly, equimolar solution of benzylamine and butyric acid was incubated in 2-methyl-2-butanol and the reaction was followed by thin-layer chromatography (TLC). The final product was then purified by a silica column and characterized by mass spectrometry (m/z = 178.2) and NMR. A final overall yield of 48% was obtained. **2** was chemically synthesized from a solution of butyryl chloride, 4-nitroaniline, and pyridine (with a molar ratio of 1.2:1:2) in anhydrous dichloromethane. The product was purified by the silica column, and it was finally characterized by NMR. The overall yield was 74%.

Kinetic parameters of amidase reaction were determined for both substrates (see the Supporting Information for details). Only summarizing here, kinetic assays were performed with the commercial free form of CALB. Reactions were carried out at increasing concentrations of substrates in 20 mM phosphate buffer at pH 7 and 37 °C with 10% organic solvent due to the poor solubility of substrates. The progression of the reaction was followed by high-performance liquid chromatography (HPLC) in the case of substrate **1** and by spectrophotometric techniques (increment of the absorbance at 405 nm) in the case of substrate **2**.

RESULTS AND DISCUSSION

Hydrolysis of the Amide Bond of 1 Catalyzed by CALB. As mentioned, the first goal of this work is to study the substrate promiscuity in the hydrolysis of the amide bond catalyzed by CALB. The exploration of the differences in the kinetics over two substrates can lead to find the key features that control the reaction rate that will serve as a starting point to obtain more efficient biocatalysts. Thus, first, the hydrolysis of the amide bond of substrate **1** was studied by kinetic experiments and by computational methods. This compound is a vanillyl derivative that was previously proposed by López-Munguia[23] and co-workers but no kinetic constants were reported, so no experimental data was available to be directly compared with theoretical results.

QM/MM Simulations. Following the molecular mechanism suggested for the primary reaction of CALB,[18] the first step of

DOI: 10.1021/acscatal.9b04002
ACS Catal. 2020, 10, 1938−1946

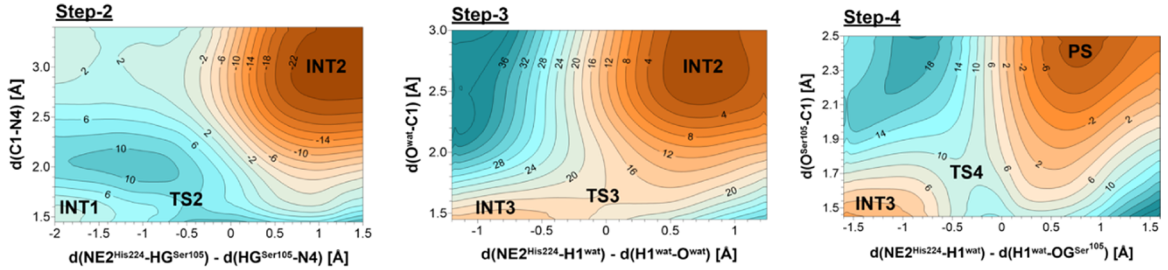

Figure 4. 2D-PMFs surfaces for the hydrolysis of **2** obtained at the M06-2X:AM1/MM level of theory. The surfaces represent the last three steps of the reaction, as depicted in Figure 5. Distances are in ångstroms, and energies of isoenergetic lines are in kcal mol^{-1}.

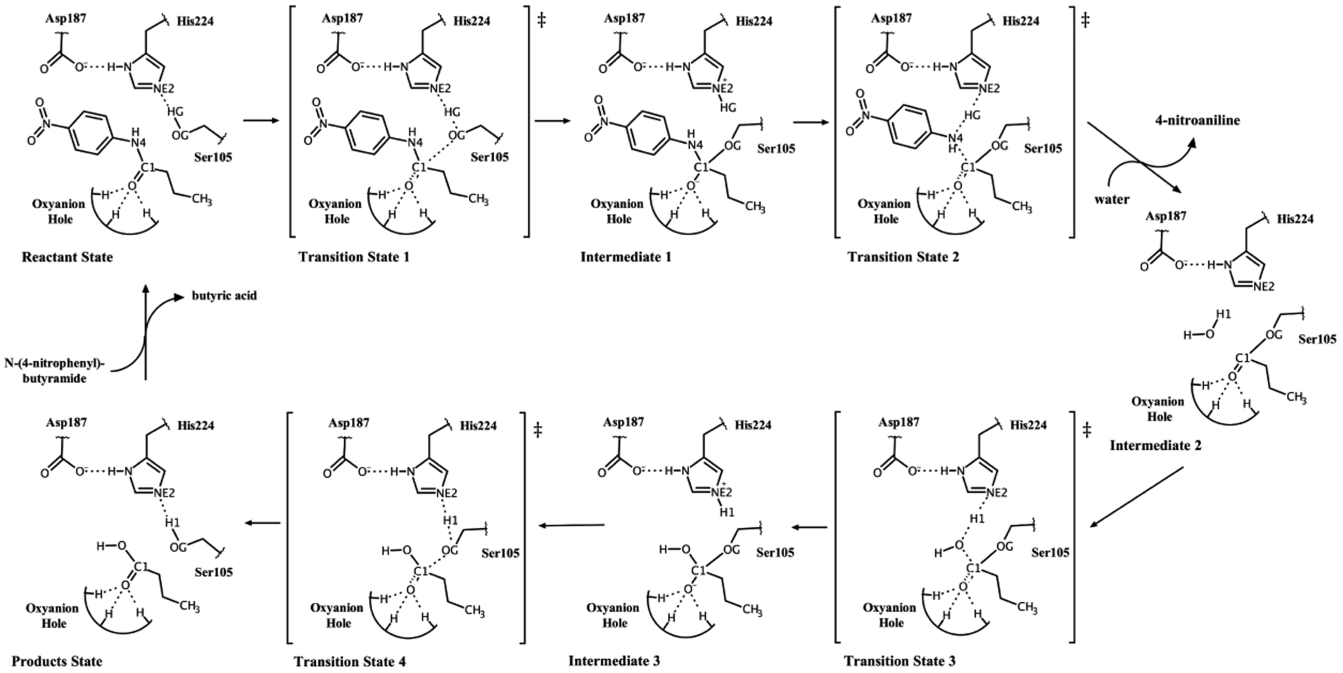

Figure 5. Schematic representation of the hydrolysis of the **2** catalyzed by CALB. The reaction yields a molecule of 4-nitroaniline (second step, INT2) and butyric acid (last step, product state).

the enzymatic hydrolysis of **1** is proposed to involve the attack of the catalytic Ser105 to the carbonyl carbon of the amide. The FES of this chemical step, computed in terms of 2D-PMF at the M06-2X:AM1/MM level, is depicted in Figure 3A, and its corresponding free energy profile in Figure 3C. In this step, the His224 residue acts as a base, allowing the activation of Ser105 and permitting consequently the formation of a tetrahedral intermediate, INT1. The negative charge of the oxygen of the amide is stabilized by strong hydrogen bond interactions in the oxyanion hole, formed by the HN of the backbone of Gln106 and Thr40, and the hydroxyl group of the lateral chain of Thr40. The FES shown in Figure 3A reveals a concerted mechanism where the transition state, TS1, is displaced close to the region of the slightly stable INT1. The free energy barrier computed for this first step is equal to 35.4 kcal mol^{-1} (Figure 3C). According to the transition state theory,[43] this barrier would correspond to a $k_{cat} = 1.9 \times 10^{-13}$ s^{-1} at 303 K. This rate constant is definitely too low for a reaction occurring in mild conditions similar to those of biological systems. Consequently, this means that the hydrolysis of the amide bond on **1** cannot take place in a reasonable time scale. Despite this computational prediction, experimental evaluation of the amidase reaction on this substrate was carried out to confirm that CALB is not capable to hydrolyze this short-acyl chain amide.

Experimental Evaluation. To assess the enzymatic hydrolysis of the amide bond, commercial wild-type CALB in its free form was used. As mentioned before, as a result of the poor solubility of **1**, 10% acetonitrile was used in the reactions. A tributyrin assay in microtiter plates was performed to confirm that CALB was active in this conditions. The reactions at increasing concentrations of substrate **1** (from 0 to 5 mM) were followed by HPLC during 48 h. The kinetic measurements reveal no hydrolysis of this substrate in any of the reactions under these conditions. Thus, this result is in agreement with the high energy barrier predicted by our QM/MM calculations.

Hydrolysis of the Amide Bond of 2 Catalyzed by CALB. To explore the amidase activity of CALB with a different substrate, the specific features of the initial substrate **1** were modified. Assuming that the efficiency of CALB can be substrate-dependent, modifications on originally used compound **1** were explored to try to find a more reactive substrate. In particular, and taking into account the character of the first step of the hydrolysis deduced from our QM/MM simulations, the inclusion of chemical groups that could increase the positive charge on the carbonyl carbon of the substrate was

DOI: 10.1021/acscatal.9b04002
ACS Catal. 2020, 10, 1938−1946

proposed. Thus, the idea was to generate a better electrophilic center on C1 position to facilitate the attack of Ser105. After analysis of possible substitutions on the benzyl ring, a nitro group was introduced in the para position, together with a shortening of the acyl chain. Prior to the complete analysis of this new substrate by experimental and QM/MM methods, the change of the charge generated by the introduced substitution on the atoms of the amide bond was computed in the gas phase, and inside the active site of the enzyme, using the CHelpG[44] method at the M06-2X level with the standard 6-31+G** basis set. The resulting maps of electrostatic potentials are shown in Figure 3D,E. These preliminary results confirmed the more positive character of the carbonyl carbon of the amide in **2**, compared to that in **1**. An increase in the negative charge on the nitrogen atom of the peptide bond is additionally observed. It is important to point out the additional electrostatic effects of the protein on the charge distribution of the substrate, as can be deduced from the comparison between the charges computed in the gas phase and in the active site of the enzyme. Thus, we proceed to study the hydrolysis of **2** catalyzed by CALB by following the same strategy as the one carried out with substrate **1**.

QM/MM Simulations. The FES of the first step of the hydrolysis of **2**, shown in Figure 3B, renders a free energy barrier of 19.5 kcal mol^{-1}, which represents a dramatic decrease of 15.9 kcal mol^{-1} with respect to **1**. As expected, this meaningful decrease can be associated with the change in the charge of the carbonyl carbon of the amide that increases the electrophilic character of the carbon atom and facilitates the attack of the Ser105. Additionally, it was also observed that INT1 is more stable than in the case of **1**. This is due to the specific interaction between the substrate and the oxyanion hole, which stabilizes the formation of the tetrahedral intermediate and the negative charge developed on the oxygen atom.

These results convert **2** into an interesting substrate to study the full mechanism of hydrolysis catalyzed by CALB. Thus, on the basis of these encouraging results, the subsequent steps of the reaction were explored. The corresponding FESs are shown in Figure 4, and a scheme of the full reaction is displayed in Figure 5. Key distances on all different states, structures of the different TSs localized at M06-2X/MM level, averaged values of key interatomic distances obtained at AM1/MM level, and a list of charges computed at DFT/MM level on the key atoms for all structures appearing along the reaction are presented in the Supporting Information.

The second step of the reaction involves the proton transfer from His224 to the nitrogen atom of the amide. This leads to the breaking of the C−N bond and the formation of the 4-nitroaniline leaving group (INT2). Interestingly, the amphoteric character of His224 is modulated by the interaction with Asp187, revealed by the analysis of the interatomic distances reported in Table S4 of the Supporting Information. Thus, the $HD1_{His224}$−$OD2_{Asp187}$ distance was significantly shorter during the first step (including reactants state, 2.02 Å) than in the second step. This result suggests that the protein adopts a conformation favoring the basic character of His224 that has to accept the proton from Ser105, originally protonated in reactants. In the second step, where His224 is releasing the proton to N4 and thus acting as an acid, this distance reaches the largest value (2.19 Å). The His224−Asp187 distance will be reduced in the third step when the former residue acts as base to abstract a proton from an active site water molecule. Finally, and perhaps unexpectedly, the protein adopts a conformation in products where, despite His224 is neutral, the distance between this two residues of the dyad is really close (2.00 Å). This suggests that the enzyme is regenerated and ready to accept again the proton from Ser105. Turning to the analysis of second step, the position of TS2 on the FES (Figure 4) reveals that the C−N bond breaking takes place almost spontaneously after the proton transfer, thus evolving to a very stable INT2. The remainder of the substrate is maintained anchored to the protein through a covalent interaction with Ser105 and a very strong hydrogen bonding network established between the O2 oxygen atom and the Thr40 and Gln106 residues.

The third and fourth steps involve the regeneration of the enzyme through the hydrolysis of the acyl−enzyme complex. The third step is initiated by the attack of a water molecule to the activated C1 atom. In fact, the charge on C1 carbon atom in INT2 is 0.82 ± 0.03 au, which is noticeably higher than its value in the gas phase, 0.78 au. As occurred in the reactant state, where the C1 atom reached a high positive value favoring the nucleophilic attack of Ser105 (Figure 3E), the protein has an active electrostatic effect in this step, making C1 a better electrophile for the attack of the water molecule in INT2. The increase of the positive charge on C1 is assisted by the polarization of the C1−O2 bond through the interactions between O2 and the oxyanion hole of the active site. As shown in Tables S4 and S5, the negative charge accumulated on O2 in INT1 (−1.104 ± 0.017 au) is stabilized by strong interactions with Gln106 and Thr40, and especially with the OH of the later, whose interatomic distance reaches one of the shortest value (1.66 Å) in INT2. The distance between C1 and N4 of the substrate in INT2 is 2.84 Å, but it is elongated up to 3.81 Å to leave space enough for the water to be correctly posed. Interestingly, the polarization of the substrate is achieved not only by the oxyanion hole (Thr40 and Gln106) but also by the contribution of the catalytic triad (Ser105, His224, and Asp187) that appears to be essential to reach the final values obtained when the full enzyme is considered into the calculations (see Table S6 of the Supporting Information). The water is anchored in the active site by a hydrogen bond interaction with His224 that, in turn, activates it for the attack to the C1 carbonyl carbon. During this process, a new tetrahedral intermediate, INT3, is formed (see Figure 5). The release of the butyric acid and the regeneration of the active site take place in the last step. Interestingly, the breaking of the bond between the acyl chain of the substrate and Ser105 (C1−OG), thus generating a molecule of butyric acid, is assisted by the transfer of the proton from His224 to Ser105.

From the free energy landscape of the whole reaction, as shown in Figure 6, we can conclude that the rate-limiting step is the regeneration of the enzyme, determined by the TS4 in the case of the amidase activity. Nevertheless, the breaking of the amide bond rendering the 4-nitroaniline (reactant state to INT2), which is the step we are experimentally monitoring since initial velocities are measured, is kinetically controlled by the second step of the reaction, in which the C−N bond of the amide is broken. This step gives a total activation free energy ($\Delta G^{\ddagger}$) of 23.1 kcal mol^{-1}, which corresponds to a k_{cat} = 1.4 × 10^{-4} s^{-1}. By comparison with the free energy profile of the primary reaction of CALB,[18] both the amidase and the esterase reaction mechanisms proceed by a four-step mechanism but, as expected, the free energy barrier of the C−N bond breaking of the substrate in the secondary reaction is noticeably higher

DOI: 10.1021/acscatal.9b04002
ACS Catal. 2020, 10, 1938−1946

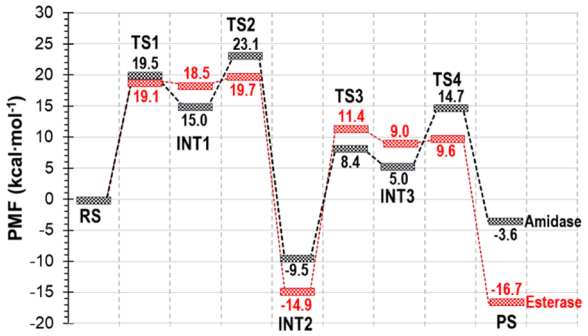

Figure 6. Free energy profile of the hydrolysis of **2** catalyzed by CALB obtained at the M06-2X:AM1/MM level (black lines). Energies are derived from the FESs displayed in Figures 3 and 4. The free energy profile of the primary reaction of CALB with **3** (Figure 3F), from ref 18, is shown by red lines.

than that of the C−O bond breaking in the primary reaction (see the red profile in Figure 6).

Experimental Evaluation. Experimental kinetics using commercial CALB was studies to confirm the predictions derived from the theoretical simulations with compound **2** as a substrate. Specific activities as a function of the concentration of substrate were fitted in a Michaelis−Menten curve. The derived kinetic constants (Table 1) were determined to be k_{cat} = (2.9 ± 0.6) × 10^{-4} s^{-1} and K_m = (4.2 ± 1.3) × 10^{-3} M. A total activation free energy of $\Delta G^{\ddagger}$ = 22.7 kcal mol^{-1} can be derived from the measured k_{cat} within the framework of the transition state theory, which is in extraordinary good agreement with the theoretical predicted value derived from the exploration of the FES ($\Delta G^{\ddagger}$ = 23.1 kcal mol^{-1}). Either theory or experiment suggests that CALB is capable to break the amide bond, but it is very dependent on specific features of the substrate. This result can be considered in agreement with kinetic studies of Bornscheuer and co-workers, who measured esterase and amidase activities of an esterase from *Bacillus subtilis* (BS2, E.C. 3.1.1.3.) on *p*-nitro-phenyl butyrate and the corresponding anilide.[45] We herein show that the impact of introducing a nitro group in the phenyl group and the shortening of the acyl chain of the substrate is dramatic on the first step of the reaction that leads to an improvement of the promiscuous amidase reaction carried out by CALB. The free energy profile, as deduced from our QM/MM calculations, shows that despite the first step is not determining the rate of the hydrolysis of the substrate the stabilization of this TS1 and the INT1 has an effect on the energy of the TS2 relative to the reactant state. In addition, the protein appears to have significant electrostatic effects on different states of the reaction as deduced from the comparison of the atomic charges in the gas phase and in the protein active site.

Table 1. Substrate Dependency on Kinetic Values of the Hydrolysis of the Amide Bond by CALB Derived from Experimental Studies[1]

substrate	benzylbutyramide (**1**)	*N*-(4-nitrophenyl)-butyramide (**2**)
V_{max} × 10^{-4} (U mg^{-1})	n/a	5.24 ± 1.07
k_{cat} × 10^{-4} (s^{-1})	n/a	2.9 ± 0.6
K_m × 10^{-3} (M)	n/a	4.2 ± 1.3
k_{cat}/K_m × 10^{-2} (M^{-1} s^{-1})	n/a	6.90 ± 2.60

[1]No activity could be determined on substrate **1**.

Kinetic Isotope Effects. To support the proposed reaction mechanism, as summarized in Figures 5 and 6, the localized TS structures at M06-2X/MM were used to compute KIEs after isotopic substitution of key heavy atoms involved in the reaction, i.e., $^{12/14}$C, $^{14/15}$N, and $^{16/18}$O of the amide bond. The use of different TSs appearing along the reaction path allows computing KIEs by assuming different possible rate-determining steps. It is important to point out that the inherent broad distribution of enzyme configurations dictates that values such as geometrical coordinates, tunneling and recrossing transmission coefficients, KIEs, etc. should be reported as ensemble averages at a certain temperature.[46] In this case, while the KIE values at a high level were obtained from a combination of a single couple of structure of TS and reactants, due to computational limitations, the use of 10 different structures of each TSs and reactants state at AM1/MM level allows obtaining an arithmetic mean and reporting the corresponding standard deviations (deposited in the Supporting Information). These suggest that the uncertainty on the M06-2X/MM values, as reported in Table 2, can be on the third decimal place.

Table 2. KIEs Computed at the M06-2X/MM Level for the Reaction of Hydrolysis of 2 Using the Different TS Structures Located along the Reaction Path

	TS1	TS2	TS3	TS4
[1-^{14}C]	1.050	1.039	1.056	1.052
[4-^{15}N]	1.009	1.017		
[2-^{18}O]	1.008	1.010	1.002	1.015

From the values of the KIEs computed at the M06-2X/MM level, the $^{12/14}$C isotopic substitution of C1 presents a normal KIE (>1) when using any of the TSs. As deduced from the scheme of the reaction depicted in Figure 5, a change of sp^2 hybridization to sp^3 on C1 occurs in TS1 and TS3, while an inverse rehybridization, sp^3 to sp^2, takes place in TS2 and TS4. Thus, an inverse ^{14}C-KIE could be expected if TS1 or TS3 was the rate-limiting step, and a normal KIE in TS2 and TS4. Nevertheless, multiple changes occur on C1 in every step. For instance, in the first step, formation of the C1−OG bond is associated with the elongation of the C1−O2 distance (from 1.26 to 1.29 Å) and an elongation of the C1−N4 bond (from 1.36 to 1.44 Å). All of these changes render a normal KIE of 5.0%. In TS3, similar changes occur and thus again a normal 5.6% KIE is observed. In TS2, the C1−N4 bond is broken and consequently a normal, and expected, effect of 3.9% is observed, the same as in the last step where the breaking of the bond between C1 and Ser105-OG governs the KIE, leading a normal 5.6% KIE. In the case of the $^{14/15}$N substitution, the force constants associated with the N4 atom are almost invariant in the first step, where the C1−N4 bond is just slightly elongated (from 1.36 Å in reactants state to 1.44 Å in TS1). Consequently, a very small 0.9% normal ^{15}N-KIE is obtained by considering the first step as the rate-limiting step. In the second step, the C1−N4 bond is broken but a hydrogen transfer takes place from His224. In all, a slightly higher normal ^{15}N-KIE of 1.7% is obtained for the second step. Since N4 belongs to the leaving group and does not participate in steps 3 and 4, no KIEs for last two steps were computed. Finally, the $^{16/18}$O substitution renders normal KIEs for any of the four TS structures selected as possible rate-determining steps. As observed in Table 2, and despite the O2−C1 bond is changing

DOI: 10.1021/acscatal.9b04002
ACS Catal. 2020, 10, 1938−1946

from double to single, or vice versa, in the different chemical steps of the proposed mechanism, a normal KIE is obtained in all cases. This can be rationalized based on the strong hydrogen bond interactions established between the O2 atom and the oxyanion hole formed by Gln106 and Thr40. In those steps where the O2−C1 bond is becoming a single bond (TS1 and TS3), the negative charge accumulated in O2 favors the establishment of stronger interactions with the oxyanion hole and, consequently, stiffer force constants that compensate the loss of the C1−O2 force constant. These results suggest that measurements of KIEs would not provide conclusive values that allow determining the rate-determining step.

Amidase vs Esterase Activity of CALB. Our computational results, summarized in Figures 5 and 6, combined with our previous study on the CALB primary reaction,[18] show how the promiscuous esterase CALB employs the same molecular mechanism to catalyze the hydrolysis of **2** as the natural ester substrate. Thus, in both cases, the reaction is initiated by the attack of the hydroxyl oxygen atom of Ser105 on the carbonyl carbon atom of the substrate, followed by the C−N or C−O bond breaking, for the amidase or esterase activity, respectively. The comparison of the free energy profiles for both reactions (Figure 6) shows how these two first steps determine the decomposition of the substrate. In the case of methyl acrylate, the relative free energy of the TS associated with the C−O bond breaking with respect to reactants was 19.7 kcal mol^{-1},[18] while in the present study, the TS of the C−N bond breaking is 23.1 kcal mol^{-1}, higher than the energy of reactants state. This result is in agreement with the experimentally evidence of a higher initial velocities of CALB for the primary reaction (as esterase) than for the secondary reaction (as amidase). The population analysis of both substrates computed in gas phase, as reported in Figure 3E,F, shows how the positive charge on C1 carbonyl carbon is significantly higher in compound **3** (0.83 au) than in **2** (0.78 au), which is in agreement with a more favorable electrophilic attack of the hydroxyl oxygen atom of Ser105 in the first step of the reaction for the primary reaction. However, the understanding of catalysis by CALB is not limited to the discussion of the electrostatic nature of the substrates in the gas phase. Once the substrates are posed in the active site of CALB, the charge of C1 atom is increased in the amide and in the ester, to 1.11 and 1.08 au, respectively. Thus, this promiscuous enzyme is able to activate both substrates, which explains its catalytic activities as esterase and amidase (despite for certain amides, as proved above). Nevertheless, the larger positive charge of C1 in the amide substrate than in the ester reveals that the higher esterase activity cannot be rationalized based on just the polarization of the substrate. The protein is also polarizing the breaking bond in the first intermediate, stabilizing the TS2 and thus facilitating the second step by an adequate charge distribution of the active site residues and a synchronized reorganization. In both cases, the positive charge on C1 atom is increased, as well as the negative charge of the departing N atom (see the Supporting Information and charges reported in ref 18). Interestingly, the electrostatic effects of the protein decomposed by residues reveal how the total effect of the enzyme is basically due to short-distance electrostatic interactions with the residues of the oxyanion hole and the catalytic triad of the active site.

CONCLUSIONS

In this work, the promiscuous amidase activity of CALB has been studied with two different short-acyl chain substrates. The results derived from experimental kinetic studies and QM/MM molecular dynamics (MD) simulations are in excellent agreement and show how the secondary activity of CALB is very dependent on specific features of the substrate. In particular, CALB can present amidase activity when introducing a nitro group into the para position of the substrate phenyl group, together with a reduction of the acyl chain. This conclusion is in agreement with the studies of Bornscheuer and co-workers[45] and Hult and co-workers,[47] who proposed compound **2** as a substrate for an esterase of *Bacillus subtilis* and for CALB, respectively. This is due to the electrophilic character of the nitro group that causes the displacement of the electrons toward the direction of the ring and the proximity of the lone pair of the aniline nitrogen to the ring that facilitates the electron delocalized into the aromatic ring. Nevertheless, our QM/MM simulations reveal the remarkable role of the protein in the catalysis by generating an electric field in the active site that polarizes and activates the substrate, as well as stabilizes the charge distribution on the rate-determining TS of the decomposition of the substrate. Our results show how arguments based on just the features of the substrate in the gas phase cannot explain the substrate dependence of the activity of CALB as amidase.[48]

CALB uses the same molecular mechanism to catalyze the secondary reaction and the primary reaction previously studied in our laboratory.[18] Our QM/MM simulations indicate that the breaking of the C−N bond of substrate **2** and the regeneration of the protein take place by a four steps mechanism, with an overall activation free energy for the decomposition of the amide molecule of 23.1 kcal mol^{-1}. This barrier is very close to the one derived from our rate constant corresponding to the measurements of the initial velocities that, within the frame of the transition state theory, gives a free energy of activation of 22.7 kcal mol^{-1}. CALB activates both kind of substrates by increasing the electrophile character of the carbonyl carbon atom, thus facilitating the attack of the Ser105 and stabilizing the negative charge developed in the oxygen atom of the original carbonyl group. In addition, the protein polarizes the scissile bond, thus reducing the free energy barrier of the following and decisive breaking bond step. Interestingly, while this is an almost a barrierless process in the primary reaction, the C−N bond breaking costs ca. 8 kcal mol^{-1}, thus explaining the different activities of CALB at short times.

QM/MM simulations show that measurements of heavy atoms KIEs would render small normal effects, which could confirm our predicted description of the reaction at the atomic level. However, they are not able to differentiate the rate-limiting step 2 from the other steps described in this mechanism.

The analysis of geometries, energies, and electronic features of the stationary states appearing along the reaction path of the hydrolysis of the natural substrate (primary reaction) or the promiscuous amide substrate (secondary reaction) explains the way CALB is catalyzing both reactions. Our computational results suggest that the barrier that determines the rate constant of the formation of the first product (the 4-nitroaniline) could be reduced by specific mutations on the protein. In particular, as deduced from the analysis of the

DOI: 10.1021/acscatal.9b04002
ACS Catal. 2020, 10, 1938−1946

corresponding FESs, mutations should be oriented in producing electrostatic effects that favor the rate-determining proton transfer from His225 to the N4 atom of the substrate that precedes the C1−N4 bond breaking. Further studies should be also focused in trying to stabilize the TSs of the second stage of the reaction (i.e., the regeneration of the enzyme) that, in both primary and secondary reaction consist in the attack of a water molecule and the departure of the acid (acrylic or butyric acid in the case of the primary or secondary reactions, respectively). In all, the present study illustrates how merging experimental and computational techniques can speed up our understanding of these complex biological catalysts and how to modify them to generate new biotechnological tools.

■ ASSOCIATED CONTENT

Supporting Information

The Supporting Information is available free of charge at https://pubs.acs.org/doi/10.1021/acscatal.9b04002.

Details of computational and experimental methods; time dependence of RMSD of backbone atoms in the equilibration MD simulations; transition state structures localized at M06-2X/MM; average KIEs and geometries of key states obtained at the AM1/MM level; charges on key atoms along the reaction at the M06-2X/MM level; NMR spectra; and kinetics of hydrolysis of *N*-(4-nitrophenyl)-butyramide (PDF)

■ AUTHOR INFORMATION

Corresponding Authors

*E-mail: eduardo.junceda@csic.es.
*E-mail: swiderek@uji.es.
*E-mail: moliner@uji.es.

ORCID

Eduardo García-Junceda: 0000-0002-2344-8743
Katarzyna Świderek: 0000-0002-7528-1551
Vicent Moliner: 0000-0002-3665-3391

Author Contributions

M.À.G. carried out all of the calculations and the kinetic experiments and E.G.-J., K.Ś., and V.M. designed the project and analyzed the results. All authors contributed to writing the manuscript.

Notes

The authors declare no competing financial interest.

■ ACKNOWLEDGMENTS

This work was supported by the Spanish Ministerio de Ciencia, Innovación y Universidades (Grant PGC2018-094852-B-C21), the Spanish Ministerio de Economía y Competitividad (Grant MAT2015-65184-C2-2-R), Universitat Jaume I (project UJI-B2017- 31), and the National Institutes of Health (Ref no. NIH R01 GM065368). K.Ś. thanks the MINECO for a Juan de la Cierva—Incorporación (ref IJCI-2016-27503) contract. M.À.G. thanks Universitat Jaume I for a doctoral FPI grant (PREDOC/2017/23). The authors acknowledge computational resources from the Servei d'Informàtica of Universitat Jaume I. The authors also thank Dr. I. Sánchez and Dr. R. Benito for technical assistance in the kinetic studies and chemical syntheses.

■ REFERENCES

(1) Humble, M. S.; Berglund, P. Biocatalytic Promiscuity. *Eur. J. Org. Chem.* **2011**, *2011*, 3391−3401.
(2) Copley, S. D. Shining a Light on Enzyme Promiscuity. *Curr. Opin. Struct. Biol.* **2017**, *47*, 167−175.
(3) Sheldon, R. A.; Brady, D. The Limits to Biocatalysis: Pushing the Envelope. *Chem. Commun.* **2018**, *54*, 6088−6104.
(4) Busto, E.; Gotor-Fernández, V.; Gotor, V. Hydrolases: Catalytically Promiscuous Enzymes for Non-Conventional Reactions in Organic Synthesis. *Chem. Soc. Rev.* **2010**, *39*, 4504−4523.
(5) Gotor-Fernández, V.; Brieva, R.; Gotor, V. Lipases: Useful Biocatalysts for the Preparation of Pharmaceuticals. *J. Mol. Catal. B: Enzym.* **2006**, *40*, 111−120.
(6) Ramirez-Escudero, M.; Molina-Espeja, P.; de Santos, G.; Hofrichter, M.; Sanz-Aparicio, J.; Alcalde, M. Structural Insights into the Substrate Promiscuity of a Laboratory-Evolved Peroxygenase. *ACS Chem. Biol.* **2018**, *13*, 3259−3268.
(7) Renata, H.; Wang, Z. J.; Arnold, F. H. Expanding the Enzyme Universe: Accessing Non-Natural Reactions by Mechanism-Guided Directed Evolution. *Angew. Chem., Int. Ed.* **2015**, *54*, 3351−3367.
(8) Bloom, J. D.; Arnold, F. H. In the Light of Directed Evolution: Pathways of Adaptive Protein Evolution. *Proc. Natl. Acad. Sci. U.S.A.* **2009**, *106*, 9995−10000.
(9) Nobeli, I.; Favia, A. D.; Thornton, J. M. Protein Promiscuity and Its Implications for Biotechnology. *Nat. Biotechnol.* **2009**, *27*, 157−167.
(10) Sánchez-Moreno, I.; Iturrate, L.; Martín-Hoyos, R.; Jimeno, M. L.; Mena, M.; Bastida, A.; García-Junceda, E. From Kinase to Cyclase: An Unusual Example of Catalytic Promiscuity Modulated by Metal Switching. *ChemBioChem* **2009**, *10*, 225−229.
(11) Molina-Espeja, P.; Viña-Gonzalez, J.; Gomez-Fernandez, B. J.; Martin-Diaz, J.; Garcia-Ruiz, E.; Alcalde, M. Beyond the Outer Limits of Nature by Directed Evolution. *Biotechnol. Adv.* **2016**, *34*, 754−767.
(12) Aharoni, A.; Gaidukov, L.; Khersonsky, O.; Gould, S. M.; Roodveldt, C.; Tawfik, D. S. The "evolvability" of Promiscuous Protein Functions. *Nat. Genet.* **2005**, *37*, 73−76.
(13) Wikmark, Y.; Humble, M. S.; Bäckvall, J. E. Combinatorial Library Based Engineering of *Candida Antarctica* Lipase a for Enantioselective Transacylation of Sec-Alcohols in Organic Solvent. *Angew. Chem., Int. Ed.* **2015**, *54*, 4284−4288.
(14) Maria, S.; Carlqvist, P.; Branneby, C.; Allnér, O.; Frise, A.; Hult, K.; Berglund, P.; Brinck, T. Direct Epoxidation in *Candida Antarctica* Lipase B Studied by Experiment and Theory. *ChemBioChem* **2008**, *9*, 2443−2451.
(15) Chen, X. Y.; Chen, G. J.; Wang, J. L.; Wu, Q.; Lin, X. F. Lipase/Acetamide-Catalyzed Carbon-Carbon Bond Formations: A Mechanistic View. *Adv. Synth. Catal.* **2013**, *355*, 864−868.
(16) Sarmah, N.; Revathi, D.; Sheelu, G.; Rani, K. Y.; Sridhar, S.; Mehtab, V.; Sumana, C. Recent Advances on Sources and Industrial Applications of Lipases. *Biotechnol. Prog.* **2018**, *34*, 5−28.
(17) Uppenberg, J.; Morgens, H.; Shamkant, P.; Alwyn, J. T. The Sequence, Crystal Structure Determination and Refinement of Two Crystal Forms of Lipase B from *Candida Antarctica*. *Structure* **1994**, *2*, 293−308.
(18) Świderek, K.; Martí, S.; Moliner, V. Theoretical Study of Primary Reaction of Pseudozyma Antarctica Lipase B as the Starting Point to Understand Its Promiscuity. *ACS Catal.* **2014**, *4*, 426−434.
(19) Buchholz, K. A Breakthrough in Enzyme Technology to Fight Penicillin Resistance-Industrial Application of Penicillin Amidase. *Appl. Microbiol. Biotechnol.* **2016**, *100*, 3825−3839.
(20) Escorcia, A. M.; Molina, D.; Daza, M. C.; Doerr, M. Acetylation of (R,S)-Propranolol Catalyzed by *Candida Antarctica* Lipase B: An Experimental and Computational Study. *J. Mol. Catal. B: Enzym.* **2013**, *98*, 21−29.
(21) Raza, S.; Fransson, L.; Hult, K. Enantioselectivity in *Candida Antarctica* Lipase B: A Molecular Dynamics Study. *Protein Sci.* **2001**, *10*, 329−338.
(22) Engström, K.; Vallin, M.; Syrén, P. O.; Hult, K.; Bäckvall, J. E. Mutated Variant of *Candida Antarctica* Lipase B in (S)-Selective

DOI: 10.1021/acscatal.9b04002
ACS Catal. 2020, 10, 1938−1946

Dynamic Kinetic Resolution of Secondary Alcohols. *Org. Biomol. Chem.* **2011**, *9*, 81−82.
(23) Torres-Gavilán, A.; Castillo, E.; López-Munguía, A. The Amidase Activity of *Candida Antarctica* Lipase B Is Dependent on Specific Structural Features of the Substrates. *J. Mol. Catal. B: Enzym.* **2006**, *41*, 136−140.
(24) Dewar, M. J. S.; Zoebisch, E. G.; Healy, E. F.; Stewart, J. J. P. Development and Use of Quantum Mechanical Molecular Models. 76. AM1: A New General Purpose Quantum Mechanical Molecular Model. *J. Am. Chem. Soc.* **1985**, *107*, 3902−3909.
(25) Zhao, Y.; Truhlar, D. G. The M06 Suite of Density Functionals for Main Group Thermochemistry, Thermochemical Kinetics, Noncovalent Interactions, Excited States, and Transition Elements: Two New Functionals and Systematic Testing of Four M06-Class Functionals and 12 Other Function. *Theor. Chem. Acc.* **2008**, *120*, 215−241.
(26) Jorgensen, W. L.; Tirado-rives, J. The OPLS Potential Functions for Proteins. Energy Minimizations for Crystals of Cyclic Peptides and Crambin. *J. Am. Chem. Soc.* **1988**, *110*, 1657−1666.
(27) Jorgensen, W. L.; Maxwell, D. S.; Tirado-Rives, J. Development and Testing of the OPLS All-Atom Force Field on Conformational Energetics and Properties of Organic Liquids. *J. Am. Chem. Soc.* **1996**, *118*, 11225−11236.
(28) Jorgensen, W. L.; Chandrasekhar, J.; Madura, J. D.; Impey, R. W.; Klein, M. L. Comparison of Simple Potential Functions for Simulating Liquid Water. *J. Chem. Phys.* **1983**, *79*, 926−935.
(29) Roux, B. The Calculation of the Potential of Mean Force Using Computer-Simulation. *Comput. Phys. Commun.* **1995**, *91*, 275−282.
(30) Thomas, A.; Jourand, D.; Bret, C.; Amara, P.; Field, M. J. Is There a Covalent Intermediate in the Viral Neuraminidase Reaction? A Hybrid Potential Free-Energy Study. *J. Am. Chem. Soc.* **1999**, *121*, 9693−9702.
(31) Poulsen, T. D.; Garcia-Viloca, M.; Gao, J.; Truhlar, D. G. Free Energy Surface, Reaction Paths, and Kinetic Isotope Effect of Short-Chain Acyl-CoA Dehydrogenase. *J. Phys. Chem. B* **2003**, *107*, 9567−9578.
(32) Torrie, G. M.; Valleau, J. P. Non-Physical Sampling Distibutions in Monte-Carlo Free-Energy Estimation - Umbrella Sampling. *J. Comput. Phys.* **1977**, *23*, 187−199.
(33) Kumar, S.; Rosenberg, J. M.; Bouzida, D.; Swendsen, R. H.; Kollman, P. A. The Weighted Histogram Analysis Method for Free-energy Calculations on Biomolecules. I. The Method. *J. Comput. Chem.* **1992**, *13*, 1011−1021.
(34) Field, M. J.; Albe, M.; Bret, C.; Proust-De Martin, F.; Thomas, A. The Dynamo Library for Molecular Simulations Using Hybrid Quantum Mechanical and Molecular Mechanical Potentials. *J. Comput. Chem.* **2000**, *21*, 1088−1100.
(35) Corchado, J. C.; Coitiño, E. L.; Chuang, Y. Y.; Fast, P. L.; Truhlar, D. G. Interpolated Variational Transition-State Theory by Mapping. *J. Phys. Chem. A* **1998**, *102*, 2424−2438.
(36) Nguyen, K. A.; Rossi, I.; Truhlar, D. G. A Dual-Level Shepard Interpolation Method for Generating Potential Energy Surfaces for Dynamics Calculations. *J. Chem. Phys.* **1995**, *103*, 5522−5530.
(37) Chuang, Y. Y.; Corchado, J. C.; Truhlar, D. G. Mapped Interpolation Scheme for Single-Point Energy Corrections in Reaction Rate Calculations and a Critical Evaluation of Dual-Level Reaction Path Dynamics Methods. *J. Phys. Chem. A* **1999**, *103*, 1140−1149.
(38) Javier Ruiz-Pernía, J. J.; Silla, E.; Tuñón, I.; Martí, S.; Moliner, V. Hybrid QM/MM Potentials of Mean Force with Interpolated Corrections. *J. Phys. Chem. B* **2004**, *108*, 8427−8433.
(39) Javier Ruiz-Pernía, J. J.; Silla, E.; Tuñón, I.; Martí, S. Hybrid Quantum Mechanics/Molecular Mechanics Simulations with Two-Dimensional Interpolated Corrections: Application to Enzymatic Processes. *J. Phys. Chem. B* **2006**, *110*, 17663−17670.
(40) Frisch, M. J.; Trucks, G. W.; Schlegel, H. B.; Scuseria, G. E.; Robb, M. A.; Cheeseman, J. R.; Scalmani, G.; Barone, V.; Mennucci, B.; Petersson, G. A.; Nakatsuji, H.; Caricato, M.; Li, X.; Hratchian, H. P.; Izmaylov, A. F.; Bloino, J.; Zheng, G.; Sonnenberg, J. L.; Hada, M.; Ehara, M.; Toyota, K.; Fukuda, R.; Hasegawa, J.; Ishida, M.; Nakajima, T.; Honda, Y.; Kitao, O.; Nakai, H.; Vreven, T.; Montgomery, J. A., Jr.; Peralta, J. E.; Ogliaro, F.; Bearpark, M.; Heyd, J. J.; Brothers, E.; Kudin, K. N.; Staroverov, V. N.; Kobayashi, R.; Normand, J.; Raghavachari, K.; Rendell, A.; Burant, J. C.; Iyengar, S. S.; Tomasi, J.; Cossi, M.; Rega, N.; Millam, J. M.; Klene, M.; Knox, J. E.; Cross, J. B.; Bakken, V.; Adamo, C.; Jaramillo, J.; Gomperts, R.; Stratmann, R. E.; Yazyev, O.; Austin, A. J.; Cammi, R.; Pomelli, C.; Ochterski, J. W.; Martin, R. L.; Morokuma, K.; Zakrzewski, V. G.; Voth, G. A.; Salvador, P.; Dannenberg, J. J.; Dapprich, S.; Daniels, A. D.; Farkas, O.; Foresman, J. B.; Ortiz, J. V.; Cioslowski, J.; Fox, D. J. *Gaussian 09*, revision E.01; Gaussian, Inc.: Wallingford, CT, 2009.
(41) Martí, S.; Moliner, V.; Tuñón, I.; Williams, I. H. QM/MM Calculations of Kinetic Isotope Effects in the Chorismate Mutase Active Site. *Org. Biomol. Chem.* **2003**, *1*, 483−487.
(42) Świderek, K.; Moliner, V. Computational Studies of *Candida Antarctica* Lipase B to Test Its Capability as a Starting Point to Redesign New Diels-Alderases. *J. Phys. Chem. B* **2016**, *120*, 2053−2070.
(43) Eyring, H. The Activated Complex in Chemical Reactions. *J. Chem. Phys.* **1935**, *3*, 107−115.
(44) Breneman, C. M.; Wiberg, K. B. Determining Atom-centered Monopoles from Molecular Electrostatic Potentials. The Need for High Sampling Density in Formamide Conformational Analysis. *J. Comput. Chem.* **1990**, *11*, 361−373.
(45) Kourist, R.; Bartsch, S.; Fransson, L.; Hult, K.; Bornscheuer, U. T. Understanding Promiscuous Amidase Activity of an Esterase from *Bacillus Subtilis*. *ChemBioChem* **2008**, *9*, 67−69.
(46) Pu, J.; Gao, J.; Truhlar, D. G. Multidimensional Tunneling, Recrossing, and the Transmission Coefficient for Enzymatic Reactions. *Chem. Rev.* **2006**, *106*, 3140−3169.
(47) Syrén, P. O.; Hendil-Forssell, P.; Aumailley, L.; Besenmatter, W.; Gounine, F.; Svendsen, A.; Martinelle, M.; Hult, K. Esterases with an Introduced Amidase-Like Hydrogen Bond in the Transition State Have Increased Amidase Specificity. *ChemBioChem* **2012**, *13*, 645−648.
(48) Świderek, K.; Pabis, A.; Moliner, V. A Theoretical Study of Carbon−Carbon Bond Formation by a Michael-Type Addition. *Org. Biomol. Chem.* **2012**, *10*, 5598−5605.

DOI: 10.1021/acscatal.9b04002
ACS Catal. 2020, 10, 1938−1946